



# Bio-nanocomposites films based on unmodified and modified thermoplastic starch reinforced with chemically modified nanoclays

M. P. Guarás<sup>1</sup>, M. Menossi<sup>1\*</sup> , A. Torres Nicolini<sup>1</sup>, V. A. Alvarez<sup>1</sup> , and L. N. Ludueña<sup>1</sup> 

<sup>1</sup>Grupo de Materiales Compuestos Termoplásticos (CoMP), Facultad de Ingeniería, Instituto de Investigaciones en Ciencia y Tecnología de Materiales (INTEMA), Universidad Nacional de Mar del Plata (UNMdP) y Consejo Nacional de Investigaciones Científicas y Técnicas (CONICET), Avenida Colón 10850, 7600 Mar del Plata, Buenos Aires, Argentina

Received: 20 October 2022

Accepted: 27 February 2023

Published online:

13 March 2023

© The Author(s), under exclusive licence to Springer Science+Business Media, LLC, part of Springer Nature 2023

## ABSTRACT

The use of polymers capable of being degraded by the action of microorganisms and/or enzymes without causing harmful effects is a strategy in waste management and environmental care. In this work, bio-nanocomposites based on thermoplastic starch (TPS) were synthesized by reactive extrusion using a twin-screw extruder. Two strategies were evaluated to reduce the disadvantages of TPS for packaging applications. First, starch was chemically modified producing the reaction of native starch with chemical reagents that introduce new functional groups to reduce the water adsorption. And two, nano-fillers were incorporated into TPS in order to enhance the mechanical and barrier properties, driving to materials with improved performance/cost ratio. The synergistic strategies of chemical modification and incorporation of modified nanoclays were also effective to reduce the dependence of properties of TPS with the environment humidity and the evolution thereof over time, which influences the performance during the service life of the product.

## Introduction

Starch is a natural polymer that has the advantage of being renewable, biodegradable, abundant and low-cost. These attributes have led to considerable interest in using starch as a raw material for the manufacture

of sustainable and biodegradable polymeric products [1]. The advantages related to sustainability are evident; however, the most important consideration for market insertion of this type of sustainable products are the comparison of its processability, properties and cost with conventional polymers [2]. Starch is a homo-polysaccharide and is constituted by D-glucose

Handling Editor: Steven Naleway.

Address correspondence to E-mail: matiasmenossi@conicet.gov.ar

E-mail Addresses: andrestorresnicolini@gmail.com; alvarezvera@gmail.com; luduenaunmdp@gmail.com

units linked by  $\alpha$ -1,4 bonds [1]. It is a heterogeneous material containing two microstructures, lineal (amylose) and branched (amylopectin), with some minor components such as proteins and lipids [3]. Due to the intermolecular hydrogen bonds between starch chains, decomposition temperature of starch is higher than melting temperature before gelatinization [4]. The use of starch as the basis for the manufacture of bioplastics requires physical modification of the starch by disruption of the crystalline structure of the granule irreversibly, either by mechanical stresses, pressure and/or temperature, in the presence of a limited amount of water (H<sub>2</sub>O) and any kind of plasticizer [5]. This process is called gelatinization, and the resulting product is thermoplastic starch (TPS) [6].

The main disadvantages exhibited by TPS are: (1) poor mechanical properties; (2) high hydrophilicity, which produces a change in properties with absorbed moisture; (3) high viscosity, which limits its processing; and (4) great susceptibility to retrogradation, the material recrystallizes over time, it becomes opaque and exhibits exudation of plasticizer to the environment. These variations are attributed to molecular rearrangement, which depends on both processing and storage conditions [7].

Numerous strategies have been evaluated to overcome these disadvantages; among them, chemical modification [8–11]. Most of the starch products used industrially have been chemically modified, with the aim of improving their physicochemical properties according to their final applications. Modifications are made to improve positive attributes, minimize disadvantages, or add new properties and functionality. Native starch (NS) can be chemically modified by producing the reaction of NS with chemical reagents that introduce new functional groups depending on the properties to be improved [5, 12]. Reactions are generally carried out in an aqueous medium, typically 30–45% solids (by weight), commonly at pH 7–12, under stirring conditions and controlled temperature. The reaction temperature should be prevented from reaching gelatinization of the starch. In this sense, this polysaccharide can be recovered after washing with H<sub>2</sub>O to remove unreacted reagents, salts or other soluble products, before final recovery in its dry form [13]. The introduction of ester groups, due to their small size, plays an internal plasticizing role and reduces the degree of crystallinity of the starch,

allowing the plasticizer molecule to penetrate more easily into molecules comprising starch to the subsequent plasticizing [14]. Numerous authors have demonstrated the advantages of derivatizing starch, showing a significant reduction in humidity sensitivity and a significant increase in thermal stability [5, 15, 16]. They suggested that chemical modification by esterification produces starch side chain growth and improves the performance of TPS for packaging applications as coating foods, stabilizers, for encapsulation, texturizers, among others. In this sense, the aim of introducing modified starches is dual: on the one side, enhances their final properties and, on the other hand, could improve performance/cost ratio in comparison with unmodified starches.

The introduction of clay nanoparticles to TPS is another strategy used to improve its properties resulting in polymeric nanocomposites with a high performance/cost ratio. Nanoclays (NCs) are the nanoparticles most widely investigated as reinforcement of different polymer matrices for a wide spectrum of applications, since they are a readily available and low-cost alternative compared to other nano-reinforcements. TPS/clay nanocomposites show significant improvements in mechanical properties [17], gas barrier properties [18] and thermal stability [17]; among others, generally for NC loading < 10% by weight.

NCS can be organo-modified increasing their interlayer distance promoting the intercalation process of the polymer chains into the silicate layers [19]. The chemical modification of NCs consists of the ion exchange between inorganic alkali cations of the clay surface with the desired organic cation [20]. NC modification is also used as a strategy to prepare functional nanocomposites. Benzalkonium chloride (a mixture of alkyl dimethyl benzyl ammonium chlorides, CBK) is a surface quaternary ammonium compound that can be used as NC organo-modifier. It is a low-cost product and widely used as an antimicrobial preservative in pharmaceuticals and clinical medicine to disinfect thermolabile material [21]. It was the first quaternary ammonium compound available on the market. It is also a H<sub>2</sub>O-miscible compound, the aqueous solution of which is slightly alkaline [22]. It has also been reported the effectiveness of CBK as an anti COVID-19 agent [23–25]. Other publications have reported the application of CBK-based disinfectants to inactivate COVID-19 [26, 27]. CBK has been used as an organic

modifier of various clays for different purposes such as enhancement of clay/polymer compatibility and tailored contaminants uptake for H<sub>2</sub>O remediation [28–31]. All these reported clay-modifications with CBK have been developed at laboratory scale, with long periods of reaction times from 30 min to 24 h. In recent work, we reported the whole optimized preparation of bentonite (BENT) organo-modified with CBK at pilot scale and use poly( $\epsilon$ -caprolactone) as a matrix [32]. On the other hand, there already exist different studies that analyzed binary blends based on: TPS with different clay composites [33]; TPS with different BENT contents [34]; storage time of starch/BENT nanocomposites and their properties [35]; effect of different clays on TPS biodegradability rate [36]; and, starches with chemical modifications and BENT nanocomposites [18]. However, none of these works cover and compare the effect of introducing BENT and organo-modified BENT into TPS and modified thermoplastic starch (MTPS) on their final micro- and macroscopic properties and their changes over time.

The aim of this study was to develop a processing procedure at pilot scale to obtain low-cost biostrategies that combined preparation of nanocomposites with natural and organo-modified clays, using modified and unmodified-TPS as matrices.

## Materials and methods

### Materials

Maize starch, named NS, was purchased from Distribuidora Dos Hermanos (Mar del Plata, Argentina). The shape of its granules was oval to polyhedral and it had an apparent amylose content of  $\sim 19\%$  [37]. Glycerol (GL) 99% in purity and distilled H<sub>2</sub>O (DW) were used as plasticizers and purchased from Química DEM (Mar del Plata, Argentina). Stearic acid (EA) was supplied by SA Shuchardt Merck OHG and was used as a lubricant agent for processing. The chemical modification of the starch by esterification was carried out with maleic anhydride and acetone solution both provided by Anedra in analytical grade. Raw BENT NC, from Neuquén, Argentina, was supplied by Minarmco S.A. and its cation exchange capacity (CEC) was 105 mequiv/100 g. It was mainly constituted by montmorillonite with quartz and feldspar as major impurities, and traces of

gypsum and sepiolite [38]. CBK, a quaternary ammonium salt with a long chain length between 12 and 16 carbon atoms and a benzene ring, was selected as organic modifier of Bent. It was purchased from Química Bolivar, Mar del Plata, Argentina (80 wt.% aqueous solution). The procedure of NS and NCs modifications was carried out following Cyras et al. [39] and Rivas-Rojas et al. [32] methodologies, respectively. With respect to the degree of substitution (DS) of NS, it was calculated by titration following the method reported by Zuo and co-workers [5]. DS was  $0.011 \pm 0.001$ . Xing et al. [40] reported similar values for maleated corn starch. Regarding chemical modification of BENT, the result was named BCBK. The reaction time of this procedure is the shortest reported in the literature for similar clay modifications [28–31]. More specifications about these procedures are found in supplementary information.

### Samples preparation

TPS, MTPS and their nanocomposites with BENT and BCBK were prepared by twin screw reactive extrusion. In a previous work, we optimized the materials formulation and extrusion conditions for the preparation of TPS [7, 41]. The optimal balance between gelatinization and retrogradation behavior and thermal and mechanical properties was obtained for TPS prepared with 69.5 wt.% of NS dried at 60°C for 24 h, 0.5 wt.% of EA and 30 wt.% of plasticizers. The plasticizer composition was 90 wt.% of GL and 10 wt.% of H<sub>2</sub>O. These materials were premixed in a beaker at room temperature and then feed into the main hopper of a twin-screw extruder “Doble Argentina” with bore barrel 25 mm in diameter and 950 mm in length with a die with 3 capillaries 3 mm in diameter at a screw speed of 50 rpm and temperature profile of 80/90/100/110/100 °C. In these conditions, mass flow rate was 1.5 kg/h, as other work. After extrusion, the strands  $\sim 3$  mm in diameter going out the extruder were air-cooled and guided through a cooling section to the pelletizer, 5 m away from the extruder output. This procedure was used in this work for the preparation of TPS. MTPS was also prepared by this method but changing NS by MNS (modified NS) in the materials formulation.

For the preparation of the nanocomposites, a solvent-assisted NC dispersion technique was used as a

processing strategy to improve the clay dispersion degree in nanocomposites. NCs, prior to extrusion, were dried at 60 °C for 24 h and then dispersed in the plasticizer (GL + H<sub>2</sub>O). The hydrophilic nature of BENT and plasticizers aid the dispersion process in the beaker. The CBK modifier is a hygroscopic product so easy dispersion of BCBK in the plasticizer was also achieved. After the NC dispersion, NS or MNS were added to the premixture and the same procedure for the preparation of the matrices TPS and MTPS was followed. Nanocomposites 3 wt.% of clay were prepared and named TPS3BENT, MTPS3BENT, TPS3BCBK and MTPS3BCBK. The percentage of clay and their formulations were selected from previous works. According to Guarás et al. [42], the incorporation of clay on TPS produces significant improvements in mechanical, barrier and thermal properties at low loading contents (lower than 10 wt.%). The performance of polymer/clay nanocomposites depends on their clay dispersion degree and content [19]. Improving the chemical compatibility between clay and polymer matrix is one of the strategies widely used in literature for enhancing clay dispersion degree for any clay content [43]. The aim of this work was to develop chemical modification routes for both clay and polymer in order to improve TPS/BENT compatibility seeking for the best clay dispersion degree of the nanocomposites. For this study, we chose a clay content of 3 wt.% because it was the optimal BENT and BCBK content in polycaprolactone-based nanocomposites [44]. In future works, we will study the effect of clay content using the optimal chemical modifications of this study.

Sheets of TPS, MTPS and their nanocomposites with dimensions 1 × 150 × 200 mm<sup>3</sup> were obtained by compression molding using a hydraulic press, following the next procedure: 10 min at 120 °C and 0 kg/cm<sup>2</sup>, 10 min at 120 °C and 50 kg/cm<sup>2</sup>, and finally mold cooling until 30 °C keeping 50 kg/cm<sup>2</sup>. These sheets were used for the characterization of the materials. With the goal to improve the understanding of this work, Fig. 1 displays, schematically, the mentioned processes and the bio-nanocomposite films developed.

## Characterization

### Nanoclays

In order to avoid the presence of H<sub>2</sub>O in the samples, NCs were dried at 60 °C in a vacuum oven until constant weight (24 hs). After that, the following micro- and macroscopic properties were analyzed.

**Fourier transformed infrared spectroscopy (FTIR)** The structural characteristics and the presence of CBK in modified BENT were studied by FTIR Genesis II. Diffuse reflectance method (DRIFT) was carried out to obtain FTIR spectra. Sixty-four scans were performed in a range of wavenumbers between 4000 and 600 cm<sup>-1</sup>.

**X-ray diffraction (XRD)** The X-Ray patterns and NCs interlayer distance ( $d_{001}$ ) were acquired in an Expert Instrument team. A Copper (CuK $\alpha$  = 1.54 Å) cathode was used. The monochromator was used at a voltage of 40 kV and a current intensity of 40 mA. All measurements were performed at a scanning rate of 1°/min and  $2\theta$  range from 1.5° to 10° by a step of 0.035°. Bragg's law was used to calculate the  $d_{001}$  of the NCs from the angular position of the diffraction peak [45].

**Water absorption (WA)** The WA essays of the NCs were tested at 90% relative humidity (RH) using a DW solution of 34 wt.% of glycerin. NCs were weighed at several times and the H<sub>2</sub>O absorption at each time was calculated by the following equation.

$$WA(t) = \frac{M_t - M_0}{M_0} * 100 \quad (1)$$

where  $M_t$  is the mass of the NC at a time  $t$  and  $M_0$  is the initial mass of the sample (dried). This essay was performed in quadruplicate.

**Thermogravimetric analysis (TGA)** TGA was used to evaluate the thermal stability of the NCs and the amount of CBK in BCBK calculated by the difference of weight loss at 900 °C between natural and modified NCs. Tests were carried out using a thermal analyzer (Model TGA Q500, Hüllhorst, Germany). Samples were heated at a constant rate of 10 °C/min from room temperature up to 900 °C under a nitrogen flow of 30 mL/min. Derivative thermogravimetric analysis (DTGA) was performed in order to

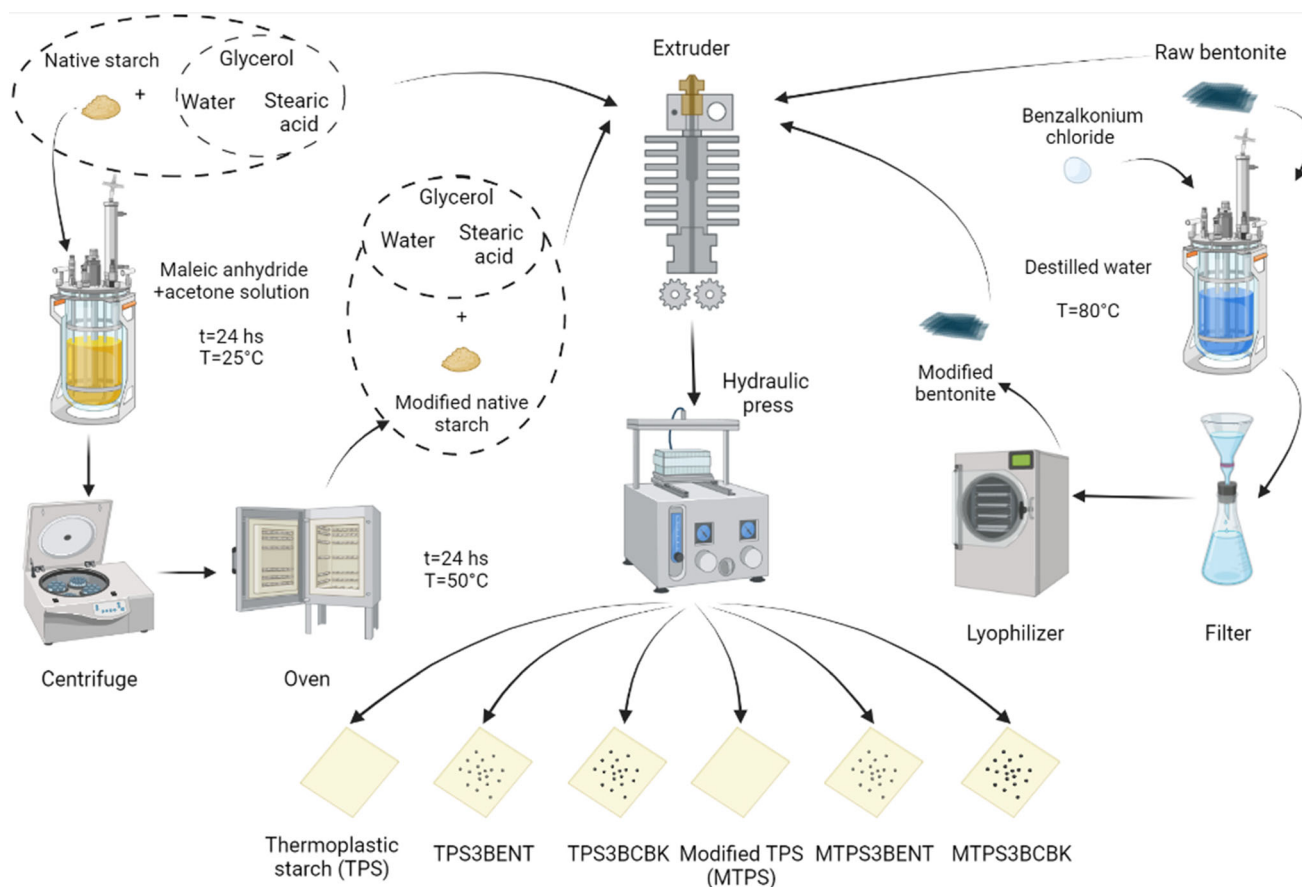


**Figure 1** Schematic process of this work, including the processes and bio-nanocomposite films developed.

identify the temperatures for the maximum thermal degradation rates of the components.

### Polymer matrices and nanocomposites

Polymer matrices and nanocomposites sheets were stored in a hermetic container at 50% of RH from the moment they were prepared. Properties were characterized at 3 storage times: 1 week ( $t_0$ ), 1 month ( $t_1$ ) and 4 months ( $t_2$ ).

**Fourier transformed infrared spectroscopy (FTIR)** FT-IR was used to analyze the presence of ester groups from maleic anhydride in MTPS. Same FT-IR test parameters as those used for NCs were used. Samples were prepared at  $t_0$ .

**Scanning electron microscopy (SEM)** SEM was used to observe the cryo-fractured surface of the samples using a JEOL JSM-6460 LV instrument. Samples were prepared at  $t_0$  by cutting 10 mm × 20 mm

rectangular specimens after their immersion in liquid air to avoid the plastic deformation of the observed surface.

**X-ray diffraction (XRD)** XRD was used to characterize the type of crystalline structure of NS and nanocomposites and its evolution as a function of storage time, as well as the dispersion of nano-reinforcements into the polymeric matrices. The tests were carried out at the same conditions as NCs but using a  $2\theta$  range between 1.5 and 60°.

**The thermogravimetric tests (TGA)** TGA essays were carried out using the same conditions as neat NCs (Sect. 3.2.1.4).

**Water adsorption (WA)** WA of the matrices and nanocomposites was performed according to the ASTM D 5229 standard. Prior to WA measurements, the samples were dried in a vacuum oven at 30–35 °C for 48 h. The samples were conditioned in hermetic containers at room temperature with 90% RH, using a

solution of glycerin and H<sub>2</sub>O. The amount of H<sub>2</sub>O absorbed by the samples was determined by weighing them periodically, until a constant weight was attained. The H<sub>2</sub>O uptake (WA) was given by Eq. 1. Three samples of each material were tested.

**Water vapor permeability (WVP)** WVP was determined following the guidelines of ASTM E96, using the Dry Method. Disks 4.9 cm diameter were cut from sheets and used to seal the open mouth of test capsules 3.9 cm in diameter and 3 cm in depth (permeation area  $\sim 18.86 \text{ cm}^2$ ), containing anhydrous calcium chloride (CaCl<sub>2</sub>) up to  $\frac{1}{4}$  of its height. Before tests, CaCl<sub>2</sub> was dried in an oven at 150 °C for 24 h (CaCl<sub>2</sub>, 0% RH). The cells were placed in a chamber at 22 °C and controlled RH (65.4% RH), and weighed daily with an analytical balance ( $\pm 0.0001 \text{ g}$ ) over a period of 5 days. The water vapor transmission (WVT) was calculated, using the following equation:

$$\text{WVT} \left[ \frac{\text{g}}{\text{h m}^2} \right] = \frac{\left( \frac{\text{G}}{t} \right)}{A} \quad (2)$$

where G/t is the slope of the weight change curve as a function of time [g/h] and A is the permeation area of the sample [m<sup>2</sup>]. Once WVT was calculated, the water vapor permeability (WVP) can be calculated using the following equation:

$$\text{WVP} \left[ \frac{\text{g}}{\text{Pa h m}} \right] = \frac{\text{WVT } e}{S * (R_1 - R_2)} \quad (3)$$

where e is the thickness of the sheet [m], S is the saturated vapor pressure at the test temperature [Pa], R<sub>1</sub> is the RH fraction of the source (for the dry method it corresponds to the humidity of the chamber) and R<sub>2</sub> is the RH fraction in the sump vapor (calcium chloride). Six measurements were made on each sample.

**The mechanical properties** Tensile properties of the sheets were measured using an INSTRON 4467 universal testing machine at 22 °C and 50% RH, according to ASTM D882. Crosshead speed of 1 mm/s and a load cell of 100 N was used. As a result, Young's Modulus (E), the maximum stress ( $\sigma_{\text{max}}$ ) and the elongation at break ( $\epsilon_r$ ) of each sample were obtained. Six measurements were made on each sample.

**Biodegradability** The biodegradation in soil of the samples was studied by evaluating weight loss (WL)

of the materials as a function of time in a soil environment. Specimens  $15 \times 15 \times 1 \text{ mm}^3$  were cut from the compression molded sheets at  $t_0$ , dried in a vacuum oven for 48 h at 35 °C, weighed and then buried in boxes with soil. Natural microflora present in soil (Pinocha type) was used as the biodegrading medium. Soil was maintained at 50% RH and samples were buried at a depth of 15 cm. Then, the samples were unearthed at 3, 5, 12, 42, 65 and 82 days, weighted to measure the H<sub>2</sub>O absorption and dried in a vacuum oven at 35 °C for 48 hs to measure the WL.

### Statistical analysis

Results are informed as mean  $\pm$  standard deviation. One-way-ANOVA with Tukey' test was used in order to establish significant differences among samples with a 95% confidence ( $p < 0.05$ ).

## Results and discussion

### Nanoclays characterization

The effectiveness of the clay modification was analyzed using FTIR. The main functional groups of BENT and BCBK are shown in in Fig. 2 and in Table 1 were summarized these functional groups with regard to their positions.

The natural BENT characteristic vibration peaks were found at 420 and 1002  $\text{cm}^{-1}$  and correspond to

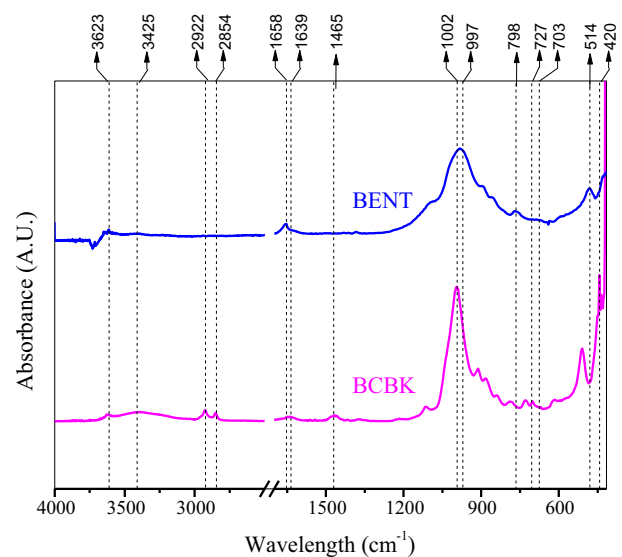


**Figure 2** FTIR spectra of BENT and BCBK samples.

**Table 1** Groups and bonds corresponding to the natural and modified bentonite absorption bands and their positions in the FTIR spectrum

Groups (bonds)	BENT (cm <sup>-1</sup> )	BCBK (cm <sup>-1</sup> )
O–H asymmetric stretching	3623	3623
O–H symmetric stretching	3425	3425
C–H asymmetric stretching	–	2922
C–H symmetric stretching	–	2854
H–O–H bending	1658	1639
Bending -CH <sub>3</sub>	–	1465
Si–O stretching	1002	997
Capa octahedral	798	798
Bending of C–H aromatic	–	727
Bending of C–H aromatic	–	703
Si–O	514	514
Si–O–Si	420	420

the clay bonds of Si–O–Si and Si–O [20]. Absorbed H<sub>2</sub>O was observed in the H–O–H bending region (1600–1700 cm<sup>-1</sup>) and also in the asymmetrical and symmetrical stretching of the O–H bonds (3100–3700 cm<sup>-1</sup>). These strips were observed in both clays [46]. The intensity of these peaks was reduced with the clay modification, due to the intercalation of quaternary salt, which modifies the surface of BENT, transforming it into a less hydrophilic surface. The CBK is hygroscopic, that is why H<sub>2</sub>O peaks are observed. When the clay was modified, the -OH present in it reacted with those present in CBK, decreasing in certain amounts the hydrophilicity of the resulting clay. The presence of CBK provided new functional groups. In this sense, characteristic peaks of CBK were those corresponding to the aromatic groups at 727 cm<sup>-1</sup> and 703 cm<sup>-1</sup>, and hydrogen-bonded methyl at 1465 cm<sup>-1</sup> [47].

The effect of BENT modification in its basal spacing was studied by XRD. The basal spacing or  $d_{001}$  of the clay was calculated from the corresponding  $2\theta$  position in the XRD patterns using the Bragg's Law [48]. It was found that the modification of the BENT with CBK increased the interlaminal spacing by 27% (Table 2). The modifier lodges on the surface of the clay sheets increasing the basal spacing, allowing the polymer chains to intercalate more easily between clay layers [49].

On the other hand, it can be observed in Table 2 that the clay modified with CBK showed a reduction of 36% in the equilibrium H<sub>2</sub>O absorption ( $WA_{eq}$ ).

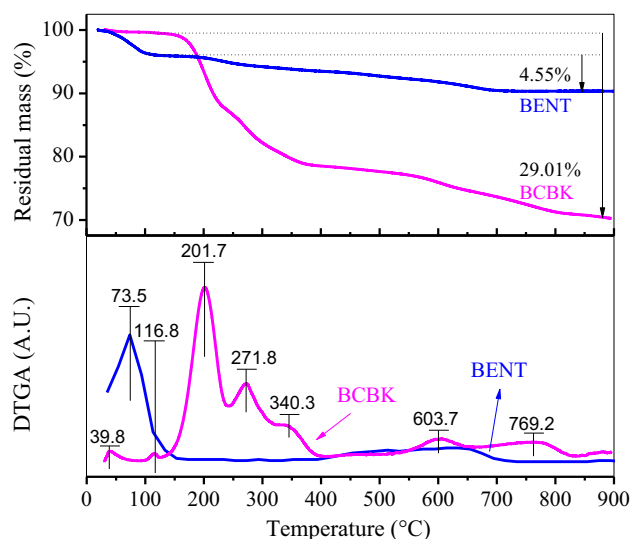
**Table 2** Interlayer distance calculated by XRD and equilibrium water absorption of nanoclays

Clay	$d_{001}$ (Å)	$WA_{eq}$ (%)
BENT	13.4	18.3 ± 0.1
BCBK	17.0	11.7 ± 0.5

When a cation with a hydrophobic tail is introduced, which electrostatically interacts with the clay in the  $d_{001}$ , it causes the organo-clay to have less affinity with H<sub>2</sub>O. This H<sub>2</sub>O property is in concordance with FT–IR analysis.

The thermal stability of clays was studied in order to evaluate the susceptibility of CBK to thermal degradation during processing. The weight loss curves (TGA) and their derivative (DTGA) as a function of temperature are shown in Fig. 3.

Figure 3 a shows the first peak between 50 °C and 120 °C corresponding to the evaporation of H<sub>2</sub>O [50]. Natural BENT showed a steeper drop in the residual mass curve as a function of temperature than BCBK in this area, which confirms the decreased H<sub>2</sub>O adsorption in BCBK. The total mass of the modifier can be calculated by the difference between the final residual mass. In this direction, the amount of CBK modifier in comparison to the total mass of BCBK was 24.46%. It is important to evaluate the thermal degradation of CBK in BCBK since, if it occurs during processing, the final properties of the

**Figure 3** TGA and DTGA curves. Weight loss and derivate weight change as a function of temperature for BENT and BCBK samples.

nanocomposites can be affected. The temperature corresponding to 10% of WL of CBK is 190°C, so thermal degradation of this component is not expected during processing using 110°C as the maximum extrusion temperature. Nevertheless, it is still necessary to have control of the temperature changes generated by shear, in order to prevent degradation [51].

## Characterization of polymer matrices and nanocomposites

### Fourier transformed infrared spectroscopy (FTIR)

The FTIR has proven to be an efficient technique for the identification of functional groups present in the chemical structure of starch and has been used in the study of chemically modified starch. Figure 4 shows the FTIR plots of the TPS and the MTPS samples.

Both spectra showed a broad peak corresponding to the stretching of the -OH bonds around 3300  $\text{cm}^{-1}$ . It was also possible to identify peaks between 1150 and 950  $\text{cm}^{-1}$ . The peak at 1150  $\text{cm}^{-1}$  was attributed to the asymmetric vibrations of the C-O-C bridge-type links, around 1100  $\text{cm}^{-1}$  the asymmetric vibrations of the C-O-C ring-type links were identified and, finally, between 1080 and 960  $\text{cm}^{-1}$  the vibrations from the stretching of the C-O bonds were observed. The peaks at 2916–2936, 1405–1465, 1245  $\text{cm}^{-1}$  were attributed to the -CH<sub>2</sub> functional

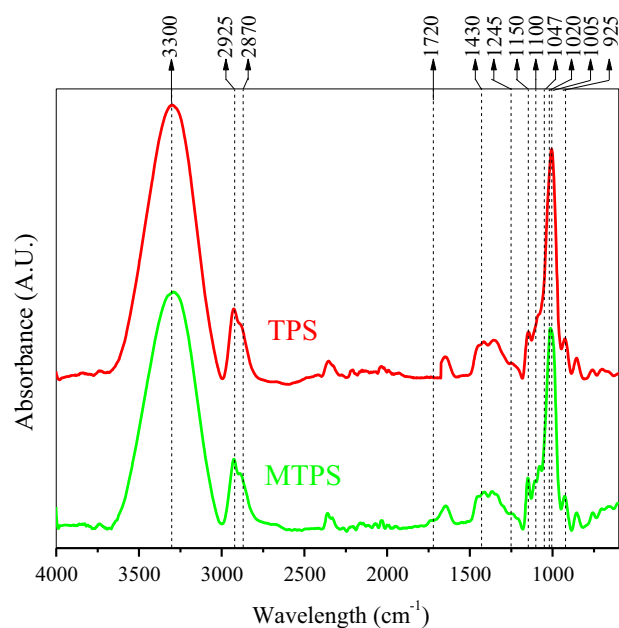


**Figure 4** FTIR spectra of TPS and MTPS samples.

groups and at 2880–2900  $\text{cm}^{-1}$  to the C-H bonds, being both characteristic peaks of polysaccharide molecules [5].

The peak in the spectrum corresponding to MTPS, located at 1720  $\text{cm}^{-1}$ , suggested the presence of ester groups belonging to maleic anhydride and confirmed the esterification of starch [52]. The peaks located at 1047 and 1020  $\text{cm}^{-1}$  were associated with the order structures and amorphous structures of starch, respectively. The ratio of intensities  $I_{1047}/I_{1020}$  was used to quantify the crystallinity index of the material [53], which are summarized in Table 3. A decrease in the crystallinity index was observed when NS was chemically modified. The same trend was reported by Cyras et al. [39] for potato starch and acetylated potato starch. This parameter was further studied by SEM and XRD techniques in the following sections. To compare the amount of -OH functional groups available in the system, the relationship between the intensity of the peak located at 3300  $\text{cm}^{-1}$  and the peak located at 1150  $\text{cm}^{-1}$  [54], associated with the vibrations corresponding to the stretching of the C-O bonds in the functional group C-OH, was used and the results are shown in Table 3. MTPS showed a decrease in available -OH. This behavior could be explained by replacing hydroxyl groups of NS by maleic anhydride, decreasing hydrogen bonds. Hu et al. [55] reported the same trend when for the esterification process and phosphate groups were incorporated through the esterification process.

This result was related to a decrease in -OH number due to the esterification reaction between the -COOH functional groups of maleic anhydride and -OH groups of GL and starch.

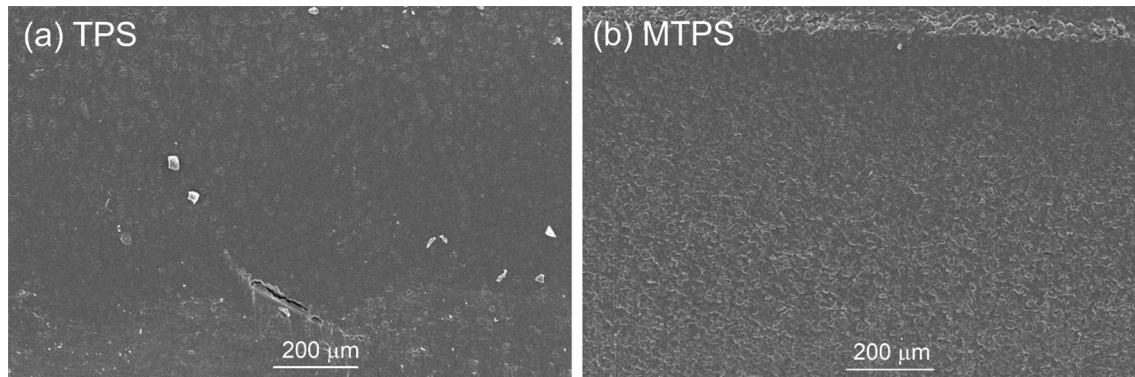
### Scanning electron microscopy (SEM)

Figure 5 shows the cryo-fractured surfaces of TPS and MTPS. These images were taken with the aim of analyzing the superficial morphology of the films. A continuous and homogeneous phase was observed in

**Table 3** Crystallinity index ( $I_{1047}/I_{1020}$ ) calculated from FT-IR spectra and calculation of available -OH functional groups of TPS and MTPS ( $I_{3300}/I_{1150}$ )

Material	$I_{1047}/I_{1020}$	$I_{3300}/I_{1150}$
TPS	0.49	5.7
MTPS	0.41	4.7





**Figure 5** Micrographs obtained by SEM of the cryo-fractured surface at  $t_0$  for: **a** TPS and **b** MTPS.

both TPS and MTPS cryo-fractured surfaces, which suggested that complete gelatinization was achieved in both cases as no residual NS granules were identified [56].

#### *X-ray diffraction (XRD)*

X-ray diffractograms were obtained, with the purpose of studying microstructural stability and monitoring the susceptibility to retrogradation of the developed nanocomposites. TPS retrogradation was analyzed by tracking the change in the material crystallinity as a function of storage time.

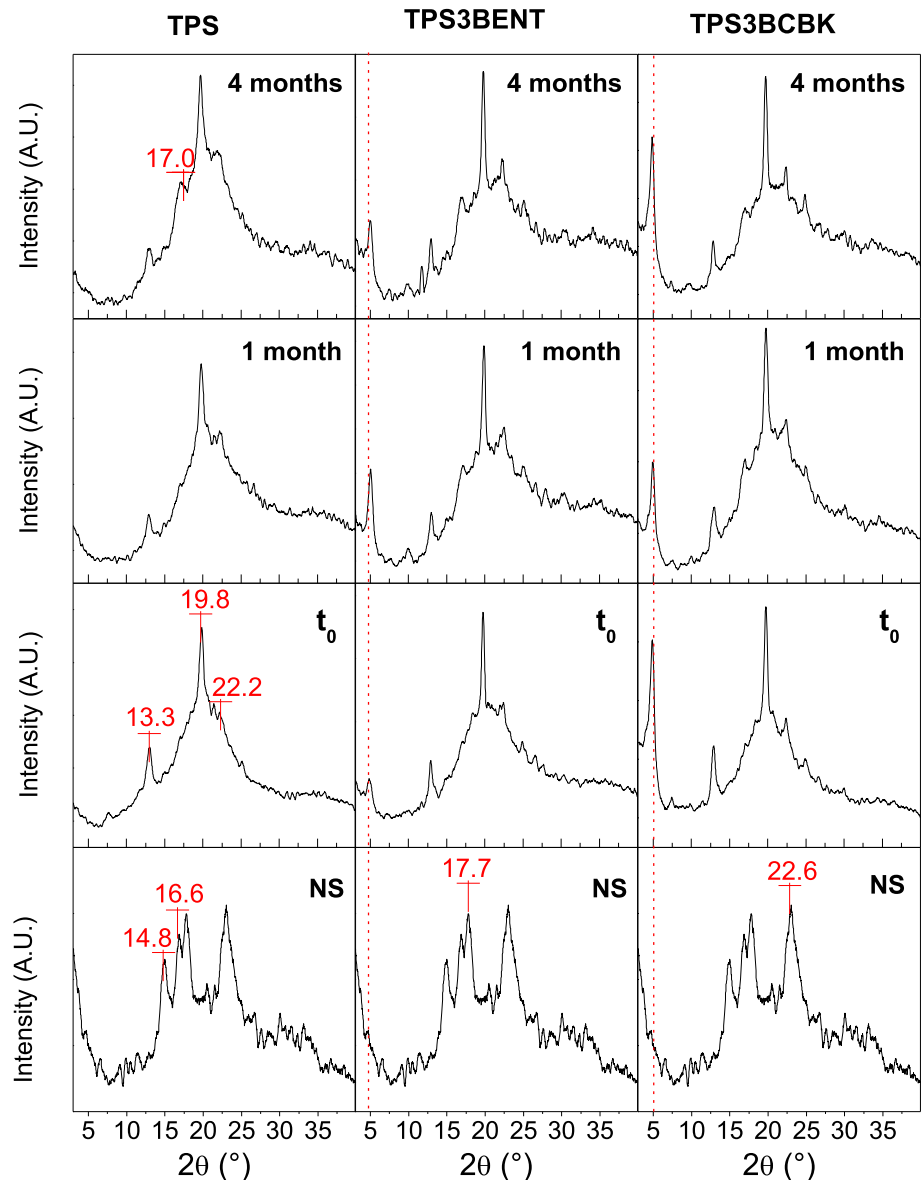
The amylose and the branched regions of amylopectin form the amorphous zone in the granule, whereas, on the other hand, amylopectin is the dominant crystalline component in NS with double helix organizations of pendant chains. Starches extracted from cereals show type-A diffractograms, starches whose source are roots and those rich in amylose present type-B diagrams; and finally, starches extracted from legumes present type-C diagrams. V-type diagrams can also be presented. This crystalline form is characterized by a single left helix with six glucose units per shift [57]. When the NS is de-structured after the gelatinization process due to the action of temperature and shear stresses; for example, by twin screw extrusion, amylose, which is an essentially linear polymer, leaves the granule and recrystallizes in different crystalline structures known as Va-type, Vh-type, and Eh-type. On the other hand, amylopectin recrystallizes in the type-B crystal structure. The type-A crystal structure of native corn starch was reported to transform into a Va-type crystal structure just after plasticization

when GL and/or H<sub>2</sub>O is used as a plasticizer, while Va-type crystals are unstable and can be transformed to Vh-type during storage, during the process known as retrogradation. Retrogradation can also be attributed to changes in the intensity of all or some peaks corresponding to the same crystal structure [58]. The NS used in this investigation showed a type-A crystalline structure, the same result was obtained by Esmaeili et al. [59] for native corn starch.

Figures 6 and 7 show the X-ray diffractograms of NS, TPS and MTPS as a function of storage time.

It was possible to identify that the intense peaks in NS and MNS at 14.8°, 16.6°, 17.7° and 22.6°, which were attributed to type-A crystalline structure [7, 60], disappeared in the gelatinized TPS and MTPS matrices and their nanocomposites at  $t_0$ . This process was attributed to transformation of the structure type-A to type-Vh after gelatinization [61]. The appearance of the intense peak at 19.8° and the peaks of medium intensity at 13.3°, 17.0° and 22.2° in the TPS and MTPS matrices and their nanocomposites was also attributed to the type-A to Vh transformation after gelatinization at  $t_0$  [7]. Although the dissimilar relative intensities and time of appearance of these peaks between MTPS and TPS samples, it can be concluded that there were not significant changes in the crystal type structure of these materials after the gelatinization process. This result was attributed to the fact that the esterification reaction has been shown to preferentially occur in the amorphous region of starch [62]. The intensity of the weak peaks at 17.0° and 22.2° for TPS, MTPS and their nanocomposites slightly increased as a function of storage time, which was attributed to progressive Vh-type crystal structure formation during

**Figure 6** X-ray patterns of NS, polymer matrices and nanocomposites as a function of storage time: TPS-based nanocomposites.

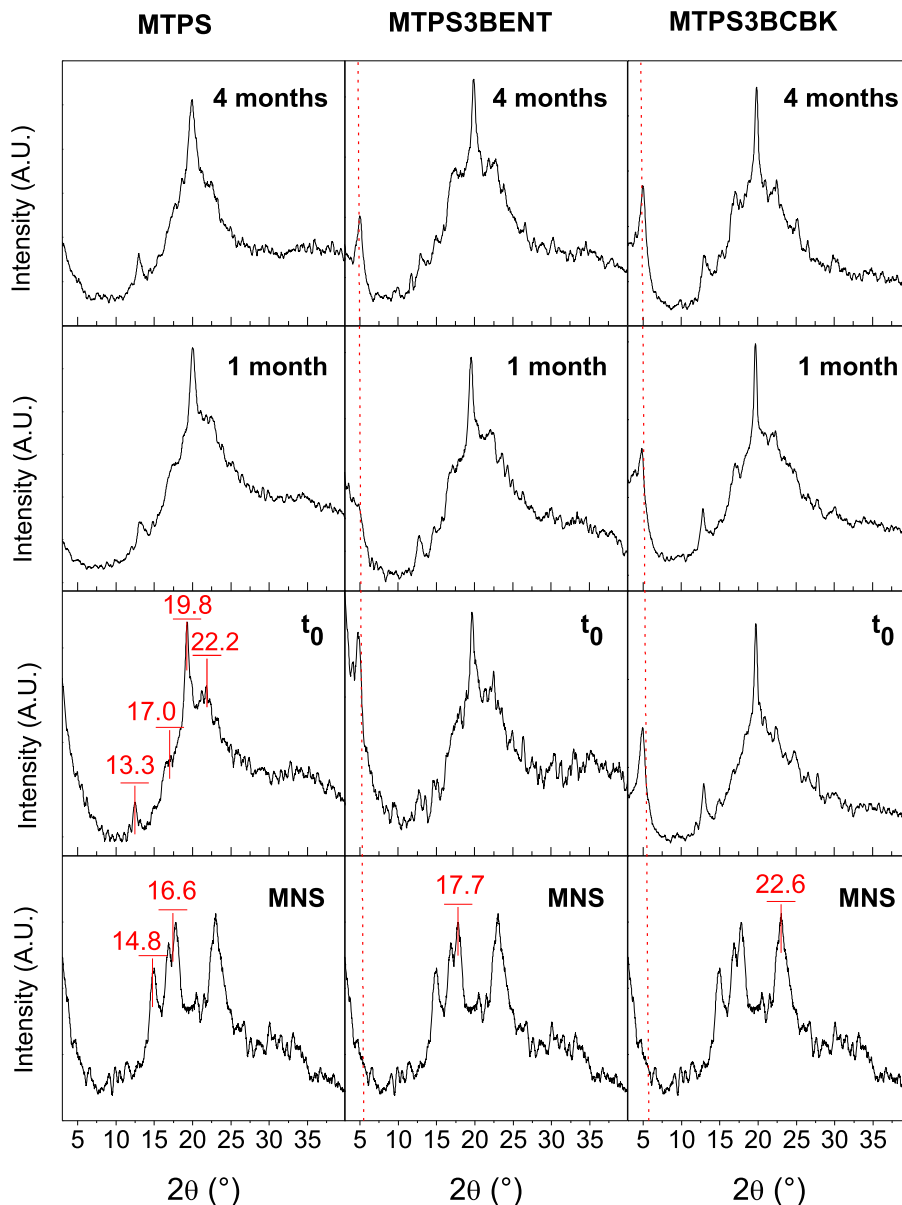


retrogradation [63]. In this direction, these results suggested that NC incorporation, BENT or BCBK, did not prevent the TPS or MTPS retrogradation over time. This behavior could be associated with the NC content. Huang et al. [64] prepared nanocomposites based on formamide/ethanolamine-plasticized TPS (FETPS) and ethanolamine-activated MMT (EMMT) as nanofillers at different weight contents: 0, 2.5, 5, 7.5 and 10%. They studied the crystallization behavior over 90 days, through XRD analysis, for the samples that contain 0 and 5 wt.% of NCS. They demonstrated that the large number of nuclei of EMMT can restrain the crystallization behavior of starch molecules in FETPS the essay.

The XRD pattern of natural Na-bentonite is given in Fig. 2. The figure indicates that the clay is composed primarily of montmorillonite, with the characteristic features at  $d_{001} = 14.29 \text{ \AA}$  and  $d_{020} = 4.49 \text{ \AA}$ .

X-ray diagrams of the nanocomposites (Figs. 6 and 7) were also useful to quantify the  $d_{001}$  of the NCs in order to analyze the structures adopted (exfoliation, intercalation and/or agglomeration) by the nano-fillers in the TPS and MTPS matrices. Natural BENT had a  $d_{001} = 13.4 \text{ \AA}$ , while  $d_{001}$  of modified BENT was  $17.0 \text{ \AA}$  (Table 2). BENT modification with CBK increased its interlaminar spacing by approximately 27%, in comparison with natural BENT. The interlaminar spacing ( $d_{001}$ ) of the NCs in each matrix can

**Figure 7** X-ray patterns of NS, polymer matrices and nanocomposites as a function of storage time: MTPS based nanocomposites.



be observed in the diffractograms in the region between  $2^\circ$  and  $10^\circ$ , denoted by the red dash line, and was calculated using Bragg's Law. Table 4 shows the  $d_{001}$  values of the nanocomposites as a function of storage time. For both clays inside the TPS and MTPS matrices, the peak corresponding to  $d_{001}$  shifted to lower angles in comparison to the neat clays but broadening of these peaks was not observed. This result suggested intercalated clay structure in all nanocomposites [44]. It was observed that the interlamellar spacing of BENT increased in the TPS matrix. This result can be attributed to the polarity of the clay, which makes it compatible with the TPS matrix promoting the intercalation process [65]. The same

trend was observed when BENT was dispersed in the MTPS matrix. Although starch modification restricts –OH groups available in the structure, the matrix remains polar and keeps its affinity with BENT. Clay modification transformed the phyllosilicate to organophilic, and this caused BCBK to decrease its affinity with the TPS matrix. It is possible to make this statement based on the fact that BCBK only slightly increased its interlamellar spacing within the nanocomposites. In the case of BCBK dispersed in MTPS, a greater increase in  $d_{001}$  was observed, probably due to the reduced polarity of the matrix and clay after the chemical modifications. The same trend was obtained by Qiao et al. [66]. They used

**Table 4** Interlayer distance (XRD), thermal stability (DTGA–TGA), water absorption (WA<sub>eq</sub>), water vapor permeability (WVP) and tensile mechanical properties of bio-nanocomposites as a function of storage time

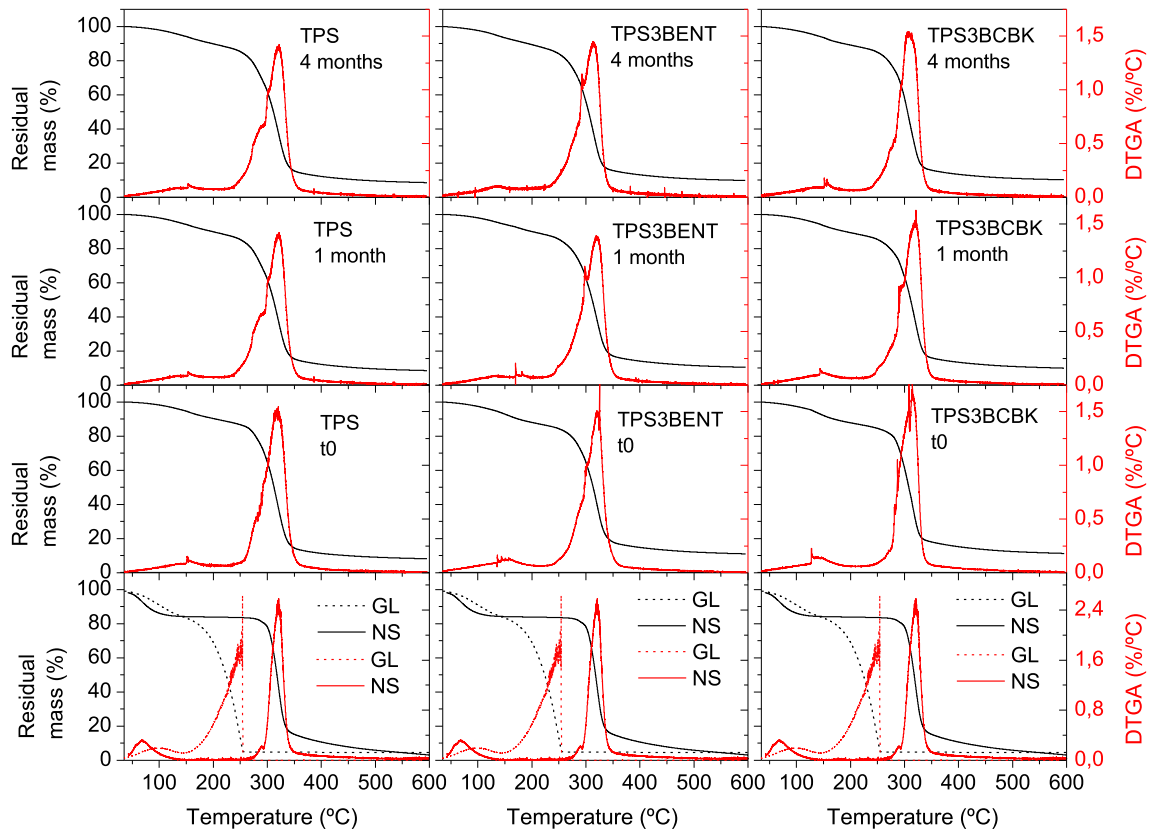
Sample	Storage time*			d <sub>001</sub> (Å)			DTGA/TGA						WA <sub>eq</sub> (%)				
	t <sub>0</sub>	t <sub>1</sub>	t <sub>2</sub>	t <sub>0</sub>	t <sub>1</sub>	t <sub>2</sub>	Tp (°C)			WL <sub>600</sub> (%)			t <sub>0</sub>	t <sub>1</sub>	t <sub>2</sub>		
							t <sub>0</sub>	t <sub>1</sub>	t <sub>2</sub>	t <sub>0</sub>	t <sub>1</sub>	t <sub>2</sub>					
NS	–	–	–	–	–	–	321.1	–	–	–	–	–	–	–	–	–	–
MNS	–	–	–	–	–	–	321.8	–	–	–	–	–	–	–	–	–	–
GL	–	–	–	–	–	–	254.2	–	–	–	–	–	–	–	–	–	–
TPS	–	–	–	–	–	–	320.8	321.2	321.1	8.2	8.6	8.5	31.2 ± 1.2 <sup>a</sup>	34.2 ± 0.1 <sup>a</sup>	36.4 ± 0.9 <sup>a</sup>		
MTPS	–	–	–	–	–	–	322.3	321.7	321.5	6.3	6.8	6.8	25.2 ± 1.2 <sup>b</sup>	27.9 ± 1.1 <sup>b</sup>	30.8 ± 1.5 <sup>b</sup>		
TPS3BENT	18.2	17.9	18.0	–	–	–	320.5	319.8	314.0	11.1	10.5	10.3	29.2 ± 0.7 <sup>acd</sup>	29.8 ± 0.1 <sup>c</sup>	28.6 ± 0.3 <sup>c</sup>		
TPS3BCBK	17.2	17.4	17.5	–	–	–	316.8	321.4	315.2	11.1	10.6	10.1	27.9 ± 1.1 <sup>cd</sup>	27.7 ± 0.1 <sup>b</sup>	26.6 ± 0.2 <sup>d</sup>		
MTPS3BENT	18.0	17.9	17.7	–	–	–	320.3	319.6	317.1	10.4	10.3	9.6	34.3 ± 1.4 <sup>c</sup>	35.2 ± 0.1 <sup>a</sup>	32.2 ± 0.9 <sup>b</sup>		
MTPS3BCBK	17.9	18.1	18.0	–	–	–	317.0	319.0	317.9	10.0	9.8	10.2	28.3 ± 1.1 <sup>d</sup>	31.2 ± 0.9 <sup>d</sup>	29.5 ± 0.4 <sup>b,c</sup>		

Sample	Storage time*			Tensile properties													
	t <sub>0</sub>	t <sub>1</sub>	t <sub>2</sub>	E (MPa)			σ <sub>max</sub> (MPa)			ε <sub>r</sub> (%)							
				t <sub>0</sub>	t <sub>1</sub>	t <sub>2</sub>	t <sub>0</sub>	t <sub>1</sub>	t <sub>2</sub>	t <sub>0</sub>	t <sub>1</sub>	t <sub>2</sub>					
NS	–	–	–	–	–	–	–	–	–	–	–	–	–	–	–	–	–
MNS	–	–	–	–	–	–	–	–	–	–	–	–	–	–	–	–	–
GL	–	–	–	–	–	–	–	–	–	–	–	–	–	–	–	–	–
TPS	1.9 ± 0.2 <sup>a</sup>	3.5 ± 0.2 <sup>a</sup>	7.9 ± 0.4 <sup>a</sup>	2.6 ± 0.1 <sup>a</sup>	25.8 ± 2.2 <sup>a</sup>	40.1 ± 2.4 <sup>a</sup>	0.8 ± 0.1 <sup>a</sup>	2.7 ± 0.1 <sup>ab,c</sup>	2.6 ± 0.5 <sup>a</sup>	86.0 ± 10.6 <sup>a</sup>	75.1 ± 6.2 <sup>a</sup>	13.8 ± 2.2 <sup>a</sup>					
MTPS	2.1 ± 0.3 <sup>a</sup>	5.2 ± 0.1 <sup>b</sup>	8.2 ± 0.2 <sup>a</sup>	7.5 ± 5.1 <sup>b</sup>	30.6 ± 7.0 <sup>ac</sup>	49.7 ± 2.1 <sup>b</sup>	1.0 ± 0.2 <sup>a</sup>	1.9 ± 0.3 <sup>b</sup>	2.0 ± 0.1 <sup>b</sup>	15.0 ± 4.0 <sup>b</sup>	12.0 ± 3.1 <sup>b</sup>	3.9 ± 0.9 <sup>b</sup>					
TPS3BENT	1.2 ± 0.1 <sup>b</sup>	1.1 ± 0.2 <sup>c</sup>	1.1 ± 0.1 <sup>b</sup>	2.0 ± 0.3 <sup>a</sup>	30.1 ± 2.9 <sup>ac</sup>	67.5 ± 5.4 <sup>c</sup>	0.9 ± 0.0 <sup>aa</sup>	3.0 ± 0.4 <sup>a</sup>	4.6 ± 0.5 <sup>cd</sup>	143.9 ± 21.7 <sup>c</sup>	60.9 ± 11.1 <sup>bc</sup>	22.8 ± 4.5 <sup>c</sup>					
TPS3BCBK	1.1 ± 0.2 <sup>b</sup>	1.0 ± 0.1 <sup>c</sup>	1.2 ± 0.1 <sup>b</sup>	2.4 ± 0.4 <sup>bc</sup>	28.3 ± 2.8 <sup>ac</sup>	58.4 ± 6.6 <sup>d</sup>	1.0 ± 0.1 <sup>a</sup>	3.0 ± 0.1 <sup>a</sup>	4.5 ± 0.4 <sup>d</sup>	111.1 ± 11.6 <sup>d</sup>	63.5 ± 6.7 <sup>a</sup>	22.8 ± 4.2 <sup>c</sup>					
MTPS3BENT	0.9 ± 0.2 <sup>b</sup>	1.1 ± 0.1 <sup>c</sup>	1.0 ± 0.2 <sup>b</sup>	7.4 ± 3.5 <sup>b</sup>	33.6 ± 1.7 <sup>bc</sup>	66.9 ± 4.8 <sup>c</sup>	0.8 ± 0.1 <sup>ac</sup>	2.1 ± 0.7 <sup>bc,d</sup>	3.4 ± 0.1 <sup>c</sup>	78.6 ± 10.0 <sup>a</sup>	47.8 ± 15.2 <sup>c</sup>	10.0 ± 0.5 <sup>a</sup>					
MTPS3BCBK	1.0 ± 0.1 <sup>b</sup>	1.2 ± 0.2 <sup>c</sup>	1.1 ± 0.2 <sup>b</sup>	2.9 ± 0.5 <sup>ac</sup>	24.5 ± 2.9 <sup>a</sup>	62.7 ± 5.8 <sup>cd</sup>	0.6 ± 0.1 <sup>bc</sup>	1.9 ± 0.1 <sup>b,d</sup>	3.6 ± 0.2 <sup>c</sup>	55.6 ± 10.1 <sup>c</sup>	35.6 ± 1.6 <sup>c</sup>	11.1 ± 2.2 <sup>a</sup>					

\* t<sub>0</sub>, 1 week; t<sub>1</sub>, 1 month; t<sub>2</sub>, 4 months

Equal letters in a column indicate that there are not statistical differences among samples (*p* < 0.05)



**Figure 8** TGA and DTGA curves. Weight loss and derivate weight change as a function of temperature for raw materials, matrices and nanocomposites as a function of storage time: TPS based nanocomposites.

montmorillonite and organically modified montmorillonite as fillers, in order to develop thermoplastic acetylated starch composites. They concluded, through layer distance, that composite based on organically modified montmorillonite and thermoplastic acetylated starch possessed better dispersion degree than montmorillonite.

Regarding storage time, significant changes of  $d_{001}$  were not observed, concluding that retrogradation did not affect the clay structure of the nanocomposites (Table 4) [56].

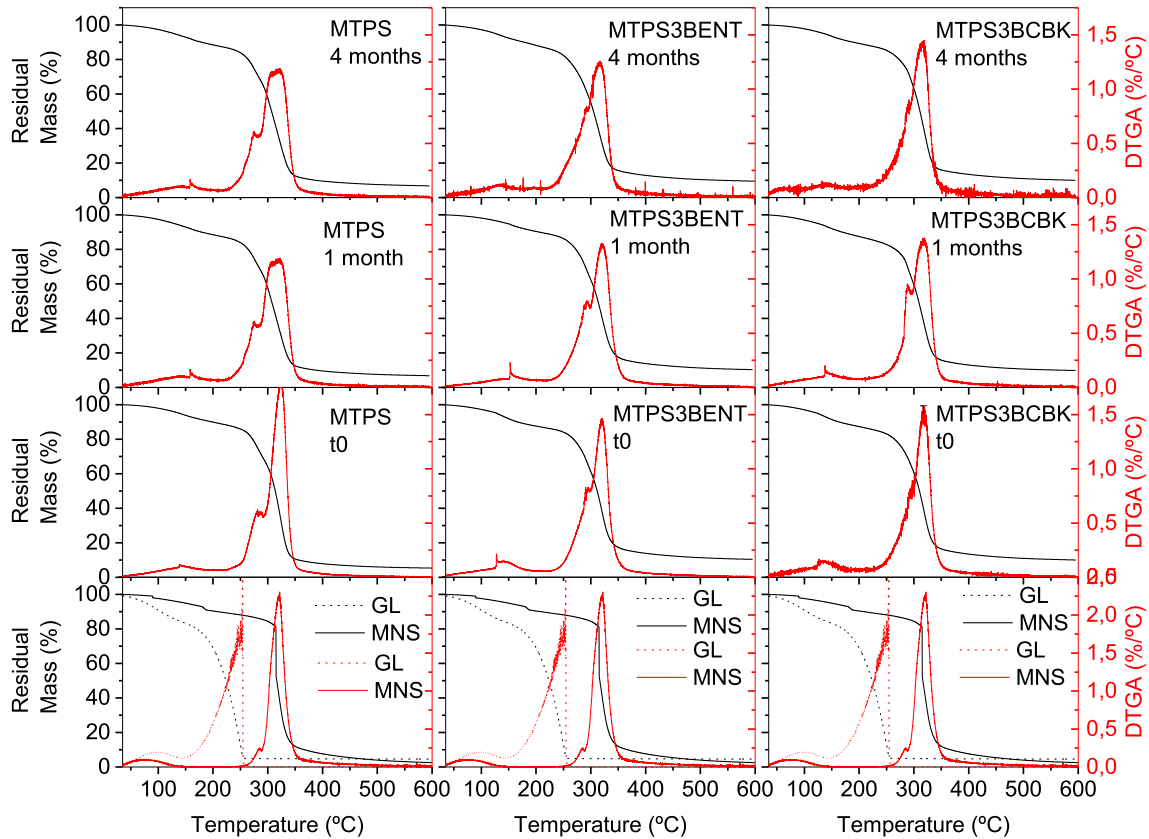
### Thermogravimetric analysis (TGA)

Figure 8 and 9 show the plots of residual mass (TGA) and its first derivative (DTGA) as a function of temperature at different storage times for raw materials, matrices and nanocomposites. The peak temperature for the main peak in the DTGA curves was named  $T_p$ . This event was associated with the maximum thermal degradation rate of starch in NS, matrices and nanocomposites and to GL evaporation in GL

curves. The residual mass at 600 °C ( $WL_{600}$ ) was calculated from the TGA curves for all samples. These values are reported in Table 4.

TPS and MTPS showed three thermal degradation steps [41]. First stage, between 80 °C and 170 °C, was attributed to the evaporation of the  $H_2O$  present in the starch structure, the  $H_2O$  absorbed from the environment and the one used as plasticizer [54]. The second stage, between 230 °C and 290 °C, was the evaporation of the GL-rich phase. During this stage, the degradation of the starch contained in the GL-rich phase also occurred [67]. The third stage was the starch degradation, that took place between 300 °C and 350 °C [62]. The starch degradation mechanism involved the elimination of polyhydroxy groups, accompanied by depolymerization and decomposition, with the final production of carbon [68, 69].

As can be observed in Table 4, all the bio-nanocomposite sheets had a higher residual mass content ( $WL_{600}$  between 9.6% and 11.1%) than the TPS and MTPS sheets ( $WL_{600}$  between 6.3% and 8.6%) after the last stage of thermal degradation. This



**Figure 9** TGA and DTGA curves. Weight loss and derivate weight change as a function of temperature for raw materials, matrices and nanocomposites as a function of storage time: MTPS based nanocomposites.

was expected since the NC silicate layers degrade at temperatures higher than 600 °C.

More specifically, it was observed that thermal stability of TPS did not show significant variations after starch chemical modification, as a function of storage time or adding NCs. The addition of nano-reinforcements did not increase the thermal stability of the matrices, but improved their  $WL_{600}$  as a function of storage time. It is possible that the nano-fillers have interacted with GL and/or  $H_2O$ , thus retarding their evaporation. These results are in agreement with X-ray essays (Sect. 3.2.3). According to Aouada et al. [70], when nano-fillers are intercalated and exfoliated into TPS matrix, a tortuous path is formed and, in consequence, could block gas and liquid channels retarding their evaporation.

**Water adsorption (WA)**

The sensitivity to moisture absorption of starch-based materials is one of the main drawbacks to overcome for biodegradable packaging applications. As can be

seen in the results reported in Table 4, MTPS showed lower  $WA_{eq}$  than TPS, which can be attributed to a decrease in  $-OH$  number due to the esterification reaction between the  $-COOH$  functional groups of maleic anhydride and  $-OH$  groups of GL and starch. These results are in concordance with FT-IR analysis and the available  $-OH$  function groups found in Sect. 3.2.1. Similar  $WA_{eq}$  values for TPS were reported by other authors [41, 71]. The chemical modification of NS, decreased the water absorption and, consequently, the films composed by this reagent. Zhang and co-workers [72] developed TPS films from different chemically modified starches. They compared the WA between MTPS and TPS, and obtained lower values for MTPS films than TPS film.  $WA_{eq}$  of both matrices, TPS and MTPS, slightly increased as a function of time which can be related to GL and/or  $H_2O$  exudation/retrogradation during the storage period. Shi et al. [73] studied TPS at different GL content and evaluated WA property during 80 days. They reported that TPS films reached a

quick value among 7 days of the essay and after 7 days, a slight change in WA was observed.

In the case of the TPS matrix nanocomposites, a slight decrease in  $WA_{eq}$  in comparison with neat TPS was observed, making this effect stronger by adding BCBK. The dispersed nano-reinforcements in the polymer matrices are expected to create a tortuous path thus decreasing the matrices' ability to absorb  $H_2O$  [74]. The reduced hydrophilicity of BCBK aids to decrease  $WA_{eq}$  in TPS/BCBK nanocomposites, in concordance with  $WA_{eq}$  of BENT and BCBK found in Sect. 3.1. The opposite trend was observed for MTPS-based nanocomposites. The  $WA_{eq}$  was higher for nanocomposites than matrix and this effect was weaker adding BCBK. This effect could be attributed to better dispersion of BENT and BCBK into the TPS matrix than the dispersion of these clays into the MTPS matrix. Mbey and co-workers [75] analyzed the influence of kaolinite content on thermoplastic cassava starch matrix and studied the  $H_2O$  uptake. They explained that a better clay intercalation is associated with a higher  $H_2O$  uptake, since it generates an increase in polymer chains mobility.

A common trend of all nanocomposites was that the susceptibility to WA did not significantly change as a function of storage time. The NCS incorporation to TPS and MTPS films may be retarding the kinetics of GL exudation.

#### *Water vapor permeability (WVP)*

The WVP of the sheets is an important parameter to avoid dehydration of fresh products or, on the other hand, the loss of crispness of dry products when the packaging material is used with the aim of avoiding moisture absorption. Biodegradable polysaccharide-based sheets are known to be an effective barrier against gas permeability, although their main disadvantage is that these materials are generally highly hydrophilic, resulting in poor barrier properties against  $H_2O$  vapor [76]. The best-known theories to explain the improvement in barrier properties with the addition of NCs in the polymer matrix are based on the theory developed by Kowalska et al. [77], which focuses on a winding path around the clay sheets, forcing the permeant ( $H_2O$  or gas) to traverse a longer path to diffuse through the sheet. According to the theory, the increase in the length of the path is a function of the high aspect ratio of the clay filler, the volumetric percentage of filler in the compound and

the degree of dispersion of the reinforcement in the polymer matrix.

The obtained WVP results are shown in Table 4. MTPS slightly increased WVP in comparison with TPS which can be a consequence of the reduced crystallinity calculated by FT-IR [78]. It is also possible to observe that the addition of nanofillers to the matrices decreased the WVP in all cases, which was caused by the decrease in the diffusivity of nanocomposites. Numerous authors [65, 79, 80] have reported in their studies, a decrease in the effective diffusion coefficient of samples containing NCs, and was associated with increased tortuosity of the system. The WVP difference between the matrices and the nanocomposites increased as a function of storage time. The matrices increase WVP as a function of storage time, while nanocomposites keep WVP almost constant. Several variables can be acting simultaneously leading to this result, among them: plasticizer exudation kinetics, retrogradation, biodegradation, polymer crystallinity,  $H_2O$  adsorption, polymer/clay-surface and polymer/clay-organo-modifier interactions, and clay  $d_{001}$ .

As we mentioned in X-ray essays (Sect. 3.2.3), the NC incorporation did not prevent the TPS or MTPS retrogradation over time; however, the presence of BENT and BCBK maintained low WVP values during the essay. These results are significantly important for the use of these nanocomposites for food packaging applications, due to the moisture content should be maintained [45].

#### *Mechanical properties*

The mechanical properties of the matrices and nanocomposites were obtained from the stress–strain curves. The following parameters were calculated from the curves: Young's modulus (E), maximum tensile strength ( $\sigma_{max}$ ) and elongation at break ( $\epsilon_r$ ). The values are reported in Table 4.

Neat TPS and MTPS samples presented significant differences in their tensile properties at initial time of essay: E increased near three times for MTPS;  $\sigma_{max}$  was 25% higher for MTPS than TPS; and  $\epsilon_r$  decreased from 86 to 15% for MTPS in comparison with TPS. These results could be attributed to the introduction of maleic anhydride into NS structure, providing higher structural integrity in the TPS matrix. Indeed, Biduski et al. [81] explained this higher structural integrity through the hydrogen bonds produced by

the presence of carbonyl and carboxyl groups in MNS with hydroxyl groups.  $E$  and  $\sigma_{\max}$  did not increase after the addition of NCs to the TPS and MTPS matrices. On the other hand, the  $\varepsilon_r$  of bio-nanocomposites was higher in comparison with neat matrices. This result can be explained by several mechanisms that could act simultaneously: (1) when the material begins to undergo retrogradation, this process causes embrittlement and reduces the elongation at break [7]; (2) the addition of NCs and their strong interaction with  $H_2O$  molecules (by ion–dipole interactions) can help retain moisture in the samples, resulting in a more plasticized material with greater elongation at break [82]; and (3) differences in clay dispersion degree and morphology at clay/polymer interface may contribute to dissimilar tendencies in mechanical properties, among them: clay modifier and the smaller polymer chains can act as slippage zones between the long polymer chains [45][83]. When GL is used as a plasticizer, it is incorporated into the starch network, decreasing direct interactions and the proximity between the starch chains. This phenomenon promotes the movements of polymer chains when tensile stresses are applied to the samples, thus improving their flexibility [56].

The  $E$  of matrices and nanocomposites increased as a function of storage time. This effect can be attributed to the evaporation of the plasticizer during storage, as was previously mentioned. On the other hand, this behavior may be also related to the retrogradation phenomenon observed by XRD essays

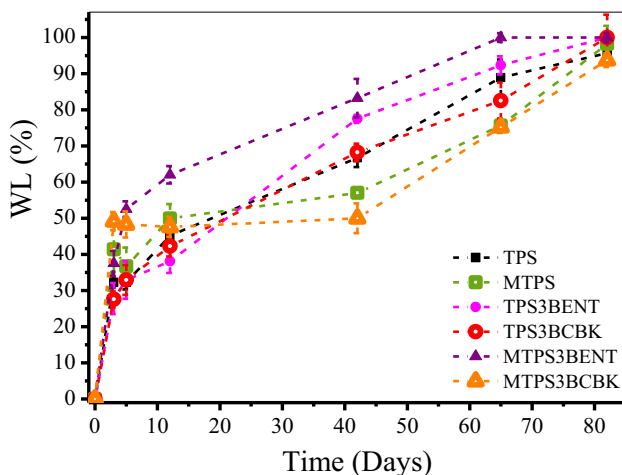


**Figure 10** Weight loss (WL) curves of TPS and MTPS based nanocomposites samples as a function of biodegradation time (days). The lines were added in order to enhance the understanding of the figure.

(Sect. 3.2.3.). TPS consists of a molecular network of semi-crystalline amylose and amylopectin with some granular segments (consisting of residual swollen granules, partially melted, deformed and broken granules, as well as recrystallized starch). With the passage of time, an increase in the number of crystalline regions acts as physical cross-linking points resulting in a reinforced network, for this reason the rigidity of the materials increases [84]. This result is further reflected in the decrease of  $\varepsilon_r$  and the increase in  $\sigma_{\max}$  of these materials as a function of time.

### Biodegradability

The biodegradation curves (WL as a function of time) of matrices and nanocomposites buried in soil are shown in Fig. 10. TPS, MTPS and their nanocomposites were removed at specific times: 3, 5, 12, 42, 65 and 82 days.

According to Merino et al. [85], the biodegradation of starch-based materials presents three stages. The first stage is related to a quick WL behavior between the first days of the essay, associated with the loss of the plasticizer; in this case, glycerol. For example, the MTPS3BCBK reached nearly 50% of WL after 5 days of soil burial. This behavior was already explained by González-Seligma and co-workers [86]. When the samples come into contact with soil, the  $H_2O$  can diffuse through them, promoting microbial development and causing swelling. Unlike formulations based on TPS, MTPS3BENT and MTPS3BCBK samples reached higher WL values, near 50%, than MTPS sample (37%). This behavior could be associated with  $H_2O$  barrier properties, more specifically,  $WA_{eq}$ . MTPS sample presented lower  $WA_{eq}$  value (25.2%) than their MTPS-based composites: MTPS3BENT (34.3%) and MTPS3BCBK (28.3%). Higher sensitivity to moisture absorption is related to higher swelling, facilitating microbial growth and, in consequence, higher WL values.

The second stage occurs between 6 and 65 days of biodegradation test. This is related to a slower degradation rate, reaching 70–90% of WL values. After the first stage, the TPS material is quickly consumed by the microbial action, which further accelerates the disintegration or fragmentation of the polymer chains, weakening the material and consequently increasing its biodegradability [87]. On the other hand, it is possible to observe that all the nanocomposites, with the exception of MTPS3BCBK,



degraded at a higher rate than their corresponding matrices. The case of the MTPS3BCBK system was correlated with the increased compatibility between the matrix and the reinforcement, which generates strong intermolecular bonds and, consequently, stronger resistance to biodegradation. Similar results were obtained by other authors [41, 85]. On the other hand, the highest biodegradation rate was shown by the MTPS3BENT nanocomposite. This result could be attributed to the incompatibility between the NC and matrix. It is also possible to observe that TPS degrades faster than MTPS which can be a consequence of the lower hydrophilicity of MTPS becoming less vulnerable to hydrolytic attack.

The last stage occurs between 65 and 82 days, and the biodegradation rate is even slower than the second stage [85]. In this stage, the molecular weight of the TPS- and MTPS-based formulations are reduced by abiotic and biotic degradation mechanisms. Most of the samples reached 100% of WL.

These results are promising for the case of food packaging, due to a quick biodegradation process for the new materials is mandatory in order to avoid plastic waste accumulation.

## Conclusions

In this study TPS/NC bio-nanocomposites have been processed by reactive extrusion. BENT NC modification was performed using a quaternary ammonium salt. The effect of adding neat BENT and modified BENT (BCBK) to matrices of TPS and MTPS was studied. A solvent-assisted twin extrusion technique at pilot scale was developed, in order to improve the dispersion degree of the clay in the nanocomposite. The effect of material properties as a function of storage time at controlled temperature and RH was evaluated.

The TPS3BCBK nanocomposite was selected as the promising material for packaging applications. It showed reduced H<sub>2</sub>O absorption and WVP. The stability of these properties, and also thermal degradation rate, during storage for 4 months was improved. In addition, it showed improved E and  $\sigma_{\max}$  and similar  $\epsilon_r$  and biodegradation rate with regard to the neat matrix. The chemical modification of NS did not lead to significant improvements on the properties of MTPS and its nanocomposites in comparison with those based on TPS. It can be concluded

that the increased time and costs involved in the chemical modification of NS was less efficient than the incorporation and chemical modification of BENT. The film blow molding processing and antimicrobial activity of TPSBCBK nanocomposites is being currently studied and will be reported in a future work.

## Acknowledgements

Authors acknowledge the collaboration of Eng. Matías Lanfranconi and Dr. Alberto Chevalier for scaling up the production of chemically modified nanoclays.

## Author contributions

Conceptualization: M.P.G.; Methodology: M.P.G., A.T.N.; Software: M.M.; Data curation: M.P.G., M.M.; Writing—original draft presentation: M.P.G., M.M., L.N.L.; Visualization: M.M.; Investigation: M.P.G., M.M., A.T.N., V.A.A.; L.N.L.; Supervision: V.A.A., L.N.L.; Validation: M.P.G., M.M.; Writing—Reviewing and Editing: V.A.A., L.N.L.

## Funding

The authors disclosed receipt of the following financial support for the research, authorship, and publication of this article: This work was supported by the “Universidad Nacional de Mar del Plata” [15/G556 and ING560/19]; and the “Agencia Nacional de Promoción Científica y Tecnológica” [PICT 2016–2055/PICT 2017–2458/PICT 2020–02207].

## Data availability

All data generated or analyzed during this study were included in this published article. Any additional information or query is available from the corresponding author on reasonable request.

## Declarations

**Conflict of interest** The authors declare that they have no known competing financial interests or

personal relationships that could have appeared to influence the work reported in this paper.

**Supplementary Information:** The online version contains supplementary material available at <http://doi.org/10.1007/s10853-023-08354-1>.

## References

- [1] Debiagi F, Léa Rita PF, Mello SM (2017) Thermoplastic starch-based blends. *Starch-based materials in food packaging*. Elsevier, pp 153–186. <https://doi.org/10.1016/B978-0-12-809439-6.00006-6>
- [2] Sanyang ML, Ilyas RA, Sapuan SM, Jumaidin R (2018) Sugar palm starch-based composites for packaging applications BT-bionanocomposites for packaging applications. In: Swain SK (ed) *Jawaid M*. Springer International Publishing, Cham, pp 125–147
- [3] Villar MA, Barbosa SE, García MA et al (2017) Starch-based materials in food packaging: processing characterization and applications. Academic Press
- [4] Pelissari FM, Ferreira DC, Louzada LB et al (2019) Chapter 10-starch-based edible films and coatings: an eco-friendly alternative for food packaging. In: Schmiele FA MBT-S (ed) *Silva Clerici MTP*. Academic Press, pp 359–420
- [5] Zuo Y, Gu J, Yang L et al (2016) Study on the preparation of maleated thermoplastic starch by reactive extrusion. *J Thermoplast Compos Mater* 29:397–409. <https://doi.org/10.1177/0892705713518809>
- [6] Zhang Y, Rempel C (2012) Retrogradation and antiplasticization of thermoplastic starch. *Thermoplast Elastom* 117–135. <https://doi.org/10.5772/35848>
- [7] Guarás MP, A AlvarezN Ludueña VL (2019) Effect of storage time, plasticizer formulation and extrusion parameters on the performance of thermoplastic starch films. *Adv Mater Lett* 10:206–214. <https://doi.org/10.5185/amlett.2019.2205>
- [8] Noorbakhsh-Soltani SM, Zerafat MM, Sabbaghi S (2018) A comparative study of gelatin and starch-based nano-composite films modified by nano-cellulose and chitosan for food packaging applications. *Carbohydr Polym* 189:48–55. <https://doi.org/10.1016/j.carbpol.2018.02.012>
- [9] Zhou W, Zhang X, Ma H et al (2021) Chemical and physical mechanism and method of preparation of thermoplastic starch. *Prog Chem* 33:1972–1982. <https://doi.org/10.7536/PC200874>
- [10] Zha D, Guo B, Li B et al (2019) Chemical and physical mechanism of water resistance for thermoplastic starch \*. *Prog Chem* 31:156–166. <https://doi.org/10.7536/PC180309>
- [11] Zha D, Zhou W, Yin P et al (2019) Ways and mechanism of Improving the mechanical properties of thermoplastic starch. *Progress Chem* 31:1044–1055. <https://doi.org/10.7536/PC181113>
- [12] Moad G (2011) Chemical modification of starch by reactive extrusion. *Prog Polym Sci* 36:218–237
- [13] Chen Q, Yu H, Wang L et al (2015) Recent progress in chemical modification of starch and its applications. *RSC Adv* 5:67459–67474. <https://doi.org/10.1039/c5ra10849g>
- [14] Morán J, Cyras V, Vázquez A, Foresti M (2011) Characterization of chemically modified potato starch films through enzymatic degradation. *J Polym Environ* 19:217–224. <https://doi.org/10.1007/s10924-010-0268-y>
- [15] Morán JI, Cyras VP, Vázquez A (2013) Preparation and characterization of three different derivatized potato starches. *J Polym Environ* 21:395–404. <https://doi.org/10.1007/s10924-012-0539-x>
- [16] Wang LF, Pan SY, Hu H et al (2010) Synthesis and properties of carboxymethyl kudzu root starch. *Carbohydr Polym* 80:174–179. <https://doi.org/10.1016/j.carbpol.2009.11.008>
- [17] Campos-Requena VH, Rivas BL, Pérez MA et al (2017) Thermoplastic starch/clay nanocomposites loaded with essential oil constituents as packaging for strawberries—in vivo antimicrobial synergy over *Botrytis cinerea*. *Postharvest Biol Technol* 129:29–36. <https://doi.org/10.1016/j.postharvbio.2017.03.005>
- [18] Breen C, Clegg F, Thompson S et al (2019) Exploring the interactions between starches, bentonites and plasticizers in sustainable barrier coatings for paper and board. *Appl Clay Sci* 183:105272. <https://doi.org/10.1016/j.clay.2019.105272>
- [19] Ludueña LN, Vázquez A, Alvarez VA (2013) Effect of the type of clay organo-modifier on the morphology, thermal/mechanical/impact/barrier properties and biodegradation in soil of polycaprolactone/clay nanocomposites. *J Appl Polym Sci* 128:2648–2657. <https://doi.org/10.1002/app.38425>
- [20] Motawie AM, Madany MM, El-Dakrory AZ et al (2014) Physico-chemical characteristics of nano-organo bentonite prepared using different organo-modifiers. *Egypt J Pet* 23:331–338. <https://doi.org/10.1016/j.ejpe.2014.08.009>
- [21] Zanini G, Ovesen R, Hansen H, Strobel B (2013) Adsorption of the disinfectant benzalkonium chloride on montmorillonite. Synergistic effect in mixture of molecules with different chain lengths. *J Environ Manage* 128C:100–105. <https://doi.org/10.1016/j.jenvman.2013.04.056>
- [22] Vaia RA, Jandt KD, Kramer EJ, Giannelis EP (1995) Kinetics of polymer melt intercalation. *Macromolecules* 28:8080–8085. <https://doi.org/10.1021/ma00128a016>
- [23] Rabenau HF, Kampf G, Cinatl J, Doerr HW (2005) Efficacy of various disinfectants against SARS coronavirus. *J Hosp*

- Infect 61:107–111. <https://doi.org/10.1016/j.jhin.2004.12.023>
- [24] Wu YC, Chen CS, Chan YJ (2020) The outbreak of COVID-19: an overview. *J Chin Med Assoc* 83:217–220. <https://doi.org/10.1097/JCMA.0000000000000270>
- [25] Zarei A, Fardood ST, Moradnia F, Ramazani A (2020) A review on coronavirus family persistency and considerations of novel type, covid-19 features. *Eurasian Chem Commun* 2(7):798–811. <https://doi.org/10.33945/SAMI/ECC.2020.7.7>
- [26] Rundle CW, Presley CL, Militello M et al (2020) Hand hygiene during COVID-19: recommendations from the american contact dermatitis society. *J Am Acad Dermatol* 1–8. <https://doi.org/10.1016/j.jaad.2020.07.057>
- [27] Wong J, Goh QY, Tan Z et al (2020) Preparing for a COVID-19 pandemic: a review of operating room outbreak response measures in a large tertiary hospital in Singapore. *Can J Anesth/J Can Anesth* 67:732–745. <https://doi.org/10.1007/s12630-020-01620-9>
- [28] Moya R, Rodríguez-Zúñiga A, Vega-Baudrit J, Álvarez V (2015) Effects of adding nano-clay (montmorillonite) on performance of polyvinyl acetate (PVAc) and urea-formaldehyde (UF) adhesives in *Carapa guianensis*, a tropical species. *Int J Adhes Adhes* 59:62–70. <https://doi.org/10.1016/j.ijadhadh.2015.02.004>
- [29] Na-Meng ZN-L (2012) Blood compatible heparin–benzalkonium modified montmorillonite /PDMS composites. *Appl Clay Sci* 70:22–27. <https://doi.org/10.1016/j.clay.2012.08.012>
- [30] Luo W, Sasaki K, Hirajima T (2015) Surfactant-modified montmorillonite by benzyloctadecyldimethylammonium chloride for removal of perchlorate. *Colloids Surf A Physicochem Eng Asp* 481:616–625. <https://doi.org/10.1016/j.colsurfa.2015.06.025>
- [31] Ilari R, Etcheverry M, Zenobi M, Zanini G (2014) Effect of the surfactant benzalkonium chloride in the sorption of paraquat and cadmium on montmorillonite. *Int J of Environment and Health* 7:70–82. <https://doi.org/10.1504/IJEN VH.2014.060127>
- [32] Rivas-Rojas PC, Ollier RP, Alvarez VA, Huck-Iriart C (2021) Enhancing the integration of bentonite clay with polycaprolactone by intercalation with a cationic surfactant: effects on clay orientation and composite tensile properties. *J Mater Sci* 56:5595–5608. <https://doi.org/10.1007/s10853-020-05603-5>
- [33] Chen B, Evans JRG (2005) Thermoplastic starch-clay nanocomposites and their characteristics. *Carbohydr Polym* 61:455–463. <https://doi.org/10.1016/j.carbpol.2005.06.020>
- [34] Lendvai L, Kmetty Á, Karger-Kocsis J (2017) Preparation and properties of thermoplastic starch/bentonite nanocomposites. *Mater Sci Forum* 885:129–134. <https://doi.org/10.4028/www.scientific.net/MSF.885.129>
- [35] Lendvai L, Sajó I, Karger-Kocsis J (2019) Effect of storage time on the structure and mechanical properties of starch/bentonite nanocomposites. *Starch Staerke* 1800123. <https://doi.org/10.1002/star.201800123>
- [36] Julinová M, Vaňharová L, Jurča M et al (2020) Effect of different fillers on the biodegradation rate of thermoplastic starch in water and soil environments. *J Polym Environ* 28:566–583. <https://doi.org/10.1007/s10924-019-01624-7>
- [37] Gutiérrez TJ, Alvarez VA (2017) Properties of native and oxidized corn starch/polystyrene blends under conditions of reactive extrusion using zinc octanoate as a catalyst. *React Funct Polym* 112:33–44. <https://doi.org/10.1016/J.REACT FUNCTPOLYM.2017.01.002>
- [38] D’Amico DA, Ollier RP, Alvarez VA et al (2014) Modification of bentonite by combination of reactions of acid-activation, silylation and ionic exchange. *Appl Clay Sci* 99:254–260. <https://doi.org/10.1016/j.clay.2014.07.002>
- [39] Cyrus VP, Zenklusen MCT, Vazquez A (2006) Relationship between structure and properties of modified potato starch biodegradable films. *J Appl Polym Sci* 101:4313–4319. <https://doi.org/10.1002/app.23924>
- [40] Xing G-X, Zhang S-F, Ben-Zhi J, Yang J-Z (2006) Microwave-assisted synthesis of starch maleate by dry method. *Starch Stärke* 58(9):464–467. <https://doi.org/10.1002/star.200600507>
- [41] Menossi M, Salcedo F, Capiel J et al (2022) Effect of starch initial moisture on thermoplastic starch film properties and its performance as agricultural mulch film. *J Polym Res* 285. <https://doi.org/10.1007/s10965-022-03150-y>
- [42] Guarás MP, Ludueña LN, Alvarez VA (2020) Recent advances in thermoplastic starch biodegradable nanocomposites. In: Kharissova OV, Martínez LMT, Kharisov BI (eds) *Handbook of nanomaterials and nanocomposites for energy and environmental applications*. Springer International Publishing, Cham, pp 1–24. [https://doi.org/10.1007/978-3-030-11155-7\\_20-1](https://doi.org/10.1007/978-3-030-11155-7_20-1)
- [43] Ludueña LN, Kenny JM, Vázquez A, Alvarez VA (2011) Effect of clay organic modifier on the final performance of PCL/clay nanocomposites. *Mater Sci Eng, A* 529:215–223. <https://doi.org/10.1016/j.msea.2011.09.020>
- [44] Ollier RP, Casado U, Torres Nicolini A et al (2021) Improved creep performance of melt-extruded polycaprolactone/organo-bentonite nanocomposites. *J Appl Polym Sci* 1–11. <https://doi.org/10.1002/app.50961>
- [45] Merino D, Ludueña LN, Alvarez VA (2018) Dissimilar tendencies of innovative green clay organo-modifier on the final properties of poly( $\epsilon$ -caprolactone) based

- nanocomposites. *J Polym Environ* 26:716–727. <https://doi.org/10.1007/s10924-017-0994-5>
- [46] Betega de Paiva L, Morales AR, Valenzuela Díaz FR (2008) Organoclays: properties, preparation and applications. *Appl Clay Sci* 42:8–24. <https://doi.org/10.1016/j.clay.2008.02.006>
- [47] Rutala WA (1996) APIC guideline for selection and use of disinfectants. *Am J Infect Control* 24:313–342. [https://doi.org/10.1016/S0196-6553\(96\)90066-8](https://doi.org/10.1016/S0196-6553(96)90066-8)
- [48] Cullity BD (1967) *Elements of X-ray Diffraction*. Addison-Wesley Publ. Co., London
- [49] Kim NH, Malhotra SV, Xanthos M (2006) Modification of cationic nanoclays with ionic liquids. *Microporous Mesoporous Mater* 96:29–35. <https://doi.org/10.1016/j.micromeso.2006.06.017>
- [50] Zhang QX, Yu ZZ, Xie XL et al (2007) Preparation and crystalline morphology of biodegradable starch/clay nanocomposites. *Polymer (Guildf)* 48:7193–7200. <https://doi.org/10.1016/j.polymer.2007.09.051>
- [51] Sessini V, Arrieta MP, Kenny JM, Peponi L (2016) Processing of edible films based on nanoreinforced gelatinized starch. *Polym Degrad Stab* 132:157–168. <https://doi.org/10.1016/j.polymdegradstab.2016.02.026>
- [52] Zuo Y, Gu J, Yang L et al (2013) Synthesis and characterization of maleic anhydride esterified corn starch by the dry method. *Int J Biol Macromol* 62:241–247. <https://doi.org/10.1016/j.ijbiomac.2013.08.032>
- [53] Cai J, Man J, Huang J et al (2015) Relationship between structure and functional properties of normal rice starches with different amylose contents. *Carbohydr Polym* 125:35–44. <https://doi.org/10.1016/j.carbpol.2015.02.067>
- [54] Gutiérrez TJ, Valencia GA (2021) Reactive extrusion-processed native and phosphated starch-based food packaging films governed by the hierarchical structure. *Int J Biol Macromol* 172:439–451. <https://doi.org/10.1016/j.ijbiomac.2021.01.048>
- [55] Hu N, Li L, Tang E, Liu X (2020) Structural, physico-chemical, textural, and thermal properties of phosphorylated chestnut starches with different degrees of substitution. *J Food Process Preserv* 1–11. <https://doi.org/10.1111/jfpp.14457>
- [56] Schmitt H, Guidez A, Prashantha K et al (2015) Studies on the effect of storage time and plasticizers on the structural variations in thermoplastic starch. *Carbohydr Polym* 115:364–372. <https://doi.org/10.1016/J.CARBPOL.2014.09.004>
- [57] Avérous L, Halley PJ (2009) Biocomposites based on plasticized starch. *Biofuels, Bioprod Bioref* 3:329–343. <https://doi.org/10.1002/bbb.135>
- [58] Shanks RA, Gunaratne LMWK (2011) Gelatinization and retrogradation of thermoplastic starch characterized using modulated temperature differential scanning calorimetry. *J Therm Anal Calorim* 106:93–99. <https://doi.org/10.1007/s10973-011-1620-8>
- [59] Esmaili M, Pircheraghi G, Bagheri R (2017) Optimizing the mechanical and physical properties of thermoplastic starch via tuning the molecular microstructure through co-plasticization by sorbitol and glycerol. *Polym Int* 66:809–819. <https://doi.org/10.1002/pi.5319>
- [60] Raquez JM, Nabar Y, Srinivasan M et al (2008) Maleated thermoplastic starch by reactive extrusion. *Carbohydr Polym* 74:159–169. <https://doi.org/10.1016/j.carbpol.2008.01.027>
- [61] Battagazzore D, Bocchini S, Nicola G et al (2015) Isosorbide, a green plasticizer for thermoplastic starch that does not retrograde. *Carbohydr Polym* 119:78–84. <https://doi.org/10.1016/j.carbpol.2014.11.030>
- [62] Jiang W, Qiao X, Sun K (2006) Mechanical and thermal properties of thermoplastic acetylated starch/poly(ethylene-co-vinyl alcohol) blends. *Carbohydr Polym* 65:139–143
- [63] Kirwan MJ, Plant S, Strawbridge JW (2011) Plastics in food packaging. In: Coles R, Kirwan M (eds) *Food and beverage packaging technology: coles/food and beverage packaging technology*. Wiley-Blackwell, Oxford, UK, pp 157–212. <https://doi.org/10.1002/9781444392180.ch7>
- [64] Huang MF, Yu JG, Ma XF, Jin P (2005) High performance biodegradable thermoplastic starch-EMMT nanoplastics. *Polymer (Guildf)* 46:3157–3162. <https://doi.org/10.1016/j.polymer.2005.01.090>
- [65] Cyras VP, Manfredi LB, Ton-That MT, Vázquez A (2008) Physical and mechanical properties of thermoplastic starch/montmorillonite nanocomposite films. *Carbohydr Polym* 73:55–63
- [66] Qiao X, Jiang W, Sun K (2005) Reinforced thermoplastic acetylated starch with layered silicates. *Starch/Staerke* 57:581–586. <https://doi.org/10.1002/star.200500421>
- [67] García NL, Ribba L, Dufresne A et al (2011) Effect of glycerol on the morphology of nanocomposites made from thermoplastic starch and starch nanocrystals. *Carbohydr Polym* 84:203–210. <https://doi.org/10.1016/j.carbpol.2010.11.024>
- [68] Zeppa C, Gouanve EE F (2009) Effect of a plasticizer on the structure of biodegradable starch/clay nanocomposites: thermal, water-sorption, and oxygen-barrier properties. *J Appl Polym Sci* 112:2044–2056
- [69] Wilhelm HM, Sierakowski MR, Souza GP, Wypych F (2003) Starch films reinforced with mineral clay. *Carbohydr Polym* 52:101–110
- [70] Aouada FA, Mattoso LHC, Longo E (2011) New strategies in the preparation of exfoliated thermoplastic starch-montmorillonite nanocomposites. *Ind Crops Prod* 34:1502–1508. <https://doi.org/10.1016/j.indcrop.2011.05.003>

- [71] Merino D, Mansilla AY, Gutiérrez TJ et al (2018) Chitosan coated-phosphorylated starch films: Water interaction, transparency and antibacterial properties. *React Funct Polym* 131:445–453. <https://doi.org/10.1016/j.reactfunctpolym.2018.08.012>
- [72] Zhang SD, Zhang YR, Zhu J et al (2007) Modified corn starches with improved comprehensive properties for preparing thermoplastics. *Starch/Staerke* 59:258–268. <http://doi.org/10.1002/star.200600598>
- [73] Shi R, Liu Q, Ding T et al (2006) Ageing of soft thermoplastic starch with high glycerol content. *J Appl Polym Sci* 103:574–586. <https://doi.org/10.1002/app>
- [74] Silvestre C, Duraccio D, Cimmino S (2011) Food packaging based on polymer nanomaterials. *Progress in Polymer Science (Oxford)* 36:1766–1782. <https://doi.org/10.1016/j.progpolymsci.2011.02.003>
- [75] Mbey JA, Hoppe S, Thomas F (2012) Cassava starch-kaolin composite film. Effect of clay content and clay modification on film properties. *Carbohydr Polym* 88:213–222. <https://doi.org/10.1016/j.carbpol.2011.11.091>
- [76] Bertuzzi MA, Castro Vidaurre EF, Armada M, Gottifredi JC (2007) Water vapor permeability of edible starch based films. *J Food Eng* 80:972–978. <https://doi.org/10.1016/j.jfoodeng.2006.07.016>
- [77] Kowalska M, Güler H, Cöckle DL (1994) Interactions of clay minerals with organic pollutants. *Sci Total Environ* 141:223–240
- [78] Monteiro MKS, Oliveira V, Santos FK et al (2017) Incorporation of bentonite clay in cassava starch films for the reduction of water vapor permeability. *Food Res Int* 637–644. <https://doi.org/10.1016/j.foodres.2017.11.030>
- [79] Müller CMO, Laurindo JB, Yamashita F (2012) Composites of thermoplastic starch and nanoclays produced by extrusion and thermopressing. *Carbohydr Polym* 89:504–510. <https://doi.org/10.1016/j.carbpol.2012.03.035>
- [80] Park HM, Li X, Jin CZ et al (2002) Preparation and properties of biodegradable thermoplastic starch/clay hybrids. *Macromol Mater Eng* 287:553–558. [https://doi.org/10.1002/1439-2054\(20020801\)287:8%3c553::AID-MAME553%3e3.0.CO;2-3](https://doi.org/10.1002/1439-2054(20020801)287:8%3c553::AID-MAME553%3e3.0.CO;2-3)
- [81] Biduski B, da Silva FT, da Silva WM et al (2017) Impact of acid and oxidative modifications, single or dual, of sorghum starch on biodegradable films. *Food Chem* 214:53–60. <http://doi.org/10.1016/j.foodchem.2016.07.039>
- [82] Dean K, Yu L, Wu DY (2007) Preparation and characterization of melt-extruded thermoplastic starch/clay nanocomposites. *Compos Sci Technol* 67:413–421. <https://doi.org/10.1016/j.compscitech.2006.09.003>
- [83] Luduena L, Bálzamo V, Vazquez A, Alvarez VA (2009) Evaluation of methods for stiffness predictions of polymer based nanocomposites: theoretical background and examples of applications (PCL-clay nanocomposites). In: Silva R VC (ed) *Nanomaterials: properties, preparation and processes*. Nova Publishers
- [84] Mali S, Grossmann MVE, García MA et al (2006) Effects of controlled storage on thermal, mechanical and barrier properties of plasticized films from different starch sources. *J Food Eng* 75:453–460. <https://doi.org/10.1016/j.jfoodeng.2005.04.031>
- [85] Merino D, Mansilla AY, Casalongué CA, Alvarez VA (2019) Effect of nanoclay addition on the biodegradability and performance of starch-based nanocomposites as mulch films. *J Polym Environ* 27:1959–1970. <https://doi.org/10.1007/s10924-019-01483-2>
- [86] González-Seligra P, Guz L, Yepes OO et al (2017) Influence of extrusion process conditions on starch film morphology. *LWT Food Sci Technol* 84:520–528. <https://doi.org/10.1016/j.lwt.2017.06.027>
- [87] Abreu AS, Oliveira M, Machado AV (2015) Effect of clay mineral addition on properties of bio-based polymer blends. *Appl Clay Sci* 104:277–285. <https://doi.org/10.1016/j.clay.2014.12.006>

**Publisher's Note** Springer Nature remains neutral with regard to jurisdictional claims in published maps and institutional affiliations.

Springer Nature or its licensor (e.g. a society or other partner) holds exclusive rights to this article under a publishing agreement with the author(s) or other rightsholder(s); author self-archiving of the accepted manuscript version of this article is solely governed by the terms of such publishing agreement and applicable law.